

The stochastic observability of simultaneous receiver and transmitter localization is studied. A mobile vehicle-mounted receiver is assumed to draw pseudorange measurements from multiple *unknown* radio frequency transmitters and to fuse these measurements through an extended Kalman filter (EKF) to simultaneously localize the receiver and transmitters together with estimating the receiver's and transmitters' clock errors. The receiver is assumed to have perfect *a priori* knowledge of its *initial* states, while the transmitters' states are unknown. It is shown that the receiver's and transmitters' clock biases are stochastically unobservable and that their estimation error variances will diverge. A lower bound on the divergence rate of the estimation error variances of the receiver's and transmitters' clock biases is derived and demonstrated numerically. Simulation and experimental results are presented for an unmanned aerial vehicle navigating without GPS signals, using pseudoranges made on unknown terrestrial transmitters. It is demonstrated that despite the receiver's and transmitters' clock biases being stochastically unobservable, the EKF produces bounded *localization* errors.

I. INTRODUCTION

Localizing unknown radio frequency (RF) transmitters is important in applications ranging from identifying rogue transmitters, such as jammers and spoofers [1], [2], to radionavigation via signals of opportunity [3], [4]. Signals of opportunity are ambient RF signals that are not intended as localization or navigation sources, such as AM/FM [5], cellular [6], [7], digital television [8], [9], and iridium [10], [11]. These signals are abundant, diverse in frequency and direction, and received with high carrier-to-noise ratio, making them an attractive alternative to global navigation satellite system (GNSS) signals. However, unlike GNSS space vehicle (SV) states, the states of signals of opportunity transmitters, namely their position and clock error states, may not be known *a priori*, in which case they must be estimated. These states may be *simultaneously* estimated alongside the vehicle-mounted receivers's position, velocity, and clock error states, which provides a self-contained

Manuscript received December 11, 2017; revised May 10, 2018; released for publication May 10, 2018. Date of publication July 16, 2018; date of current version April 11, 2019.

DOI. No. 10.1109/TAES.2018.2856318

Refereeing of this contribution was handled by A. G. Dempster.

This work was supported in part by the Office of Naval Research under Grant N00014-16-1-2305 and in part by the National Science Foundation under Grant 1751205.

Authors' address: J. J. Morales and Z. M. Kassas are with the Department of Electrical and Computer Engineering, University of California, Riverside, CA 92521 USA, (E-mail: jmor047@ucr.edu; zkassas@ieee.org). (*Corresponding author: Zaher M. Kassas.*)

solution that does not require the installation of additional infrastructure [12], [13].

This estimation problem is referred to as radio simultaneous localization and mapping (SLAM) and is analogous to the SLAM problem in robotics [14]. However, in contrast to the *static* feature map of the typical SLAM problem, which consists of static states (e.g., positions of buildings, walls, poles, trees, etc.), the radio SLAM signal landscape map consists of static states (e.g., positions of terrestrial transmitters) and dynamic stochastic states (e.g., clock bias and drift).

Observability of the SLAM problem in robotics has been extensively studied [15]–[18]. In [19], observability of the radio SLAM problem was thoroughly analyzed through a linearized deterministic observability framework, deriving conditions on the minimal *a priori* knowledge about the receivers' and/or transmitters' states for observability. In [20], a nonlinear deterministic observability framework was utilized to show that receiver-controlled maneuvers reduce the *a priori* knowledge needed to establish observability. This paper studies the observability of the radio SLAM problem in a stochastic framework to characterize the evolution of the estimation error covariance produced by an extended Kalman filter (EKF) estimating the stochastic dynamic states.

Classic deterministic observability tests do not include the statistics of the:

- 1) process noise;
- 2) measurement noise;
- 3) initial state estimate.

The EKF Riccati equation, however, which governs the time evolution of the estimation error covariance, is a function of such statistics. Therefore, a system may pass deterministic observability tests, while there may exist a combination of system statistics for which an EKF would yield estimates with unbounded estimation error variances [21]. For this reason, studying observability via a stochastic framework is of considerable importance to characterize the time evolution of the EKF's estimation error covariance.

Several stochastic observability notions have been defined in the literature. In [21] and [22], a system was said to be stochastically observable if there exists a time such that an estimator could produce a finite estimation error covariance, when no prior information about the system's state vector is available. In [23], a system was said to be estimable if in estimating its states from measurements, the posterior estimation error covariance matrix is strictly smaller than the prior state covariance matrix. In [24] and [25], the stochastic stability of the discrete-time (DT) and continuous-time EKF were studied and conditions on the initial estimation error and disturbing noise terms were specified that will guarantee bounded estimation error. In [26], stochastic observability (or estimability) was defined as an assessment of the “degree of observability.” Thus, in contrast to Boolean deterministic observability tests, stochastic observability was defined as a measure to whether an observable system is poorly estimable due to

the gradient vectors comprising the Fisher information matrix being nearly collinear. In [27], stochastic observability was used to describe the ability of the estimator to reduce the entropy of any non-trivial function of its initial state by using the measurements.

In this paper, the stochastic observability of the radio SLAM problem is studied by directly analyzing the time evolution of the estimation error covariance through the Riccati equation. The radio SLAM problem is found to be stochastically unobservable when both the receiver's and transmitters' clock biases are simultaneously estimated by showing divergence of their individual variances. The stochastic observability analysis in this paper allows for the initial estimation error covariance to be finite, unlike other existing approaches that assume infinite initial uncertainty [21], [22]. This paper makes three contributions. First, a closed-form expression for a lower bound on the time evolution of the estimation error variances of the stochastically unobservable states is derived. Second, the lower bound's divergence rate is characterized. Third, numerical and experimental results are presented demonstrating an unmanned aerial vehicle (UAV)-mounted receiver, navigating in a radio SLAM fashion by fusing pseudoranges made on unknown terrestrial signals of opportunity transmitters. It is worth noting that this paper focuses on a planar environment to simplify the analysis. Extensions to three-dimensional (3-D) environments is expected to follow straightforwardly.

The remainder of the paper is organized as follows. Section II describes the system dynamics and measurement models. Section III studies the stochastic observability of the simultaneous receiver and transmitter localization problem. Section IV presents simulation results to validate the findings of Section III. Section V provides experimental results. Concluding remarks are given in Section VI.

II. MODEL DESCRIPTION

A. RF Transmitter Dynamics Model

Each RF signal will be assumed to emanate from a spatially-stationary terrestrial transmitter, and its state vector will consist of its planar position states $\mathbf{r}_{s_m} \triangleq [x_{s_m}, y_{s_m}]^T$ and clock error states $\mathbf{x}_{\text{clk},s_m} \triangleq c [\delta t_{s_m}, \dot{\delta t}_{s_m}]^T$, where c is the speed of light, δt_{s_m} and $\dot{\delta t}_{s_m}$ are the clock bias and drift of the m^{th} RF transmitter, respectively, and $m = 1, \dots, M$, where M is the total number of RF transmitters.

The discretized RF transmitters' dynamics are given by

$$\mathbf{x}_{s_m}(k+1) = \mathbf{F}_s \mathbf{x}_{s_m}(k) + \mathbf{w}_{s_m}(k), \quad k = 1, 2, \dots,$$

where

$$\mathbf{x}_{s_m} = [\mathbf{r}_{s_m}^T, \mathbf{x}_{\text{clk},s_m}^T]^T, \quad \mathbf{F}_s = \text{diag}[\mathbf{I}_{2 \times 2}, \mathbf{F}_{\text{clk}}], \quad \mathbf{F}_{\text{clk}} = \begin{bmatrix} 1 & T \\ 0 & 1 \end{bmatrix},$$

where T is the constant sampling interval and \mathbf{w}_{s_m} is the process noise, which is modeled as a DT white noise sequence

with covariance $\mathbf{Q}_{s_m} = \text{diag}[\mathbf{0}_{2 \times 2}, c^2 \mathbf{Q}_{\text{clk}, s_m}]$, where

$$\mathbf{Q}_{\text{clk}, s_m} = \begin{bmatrix} S_{\tilde{w}_{\delta t_s, m}} T + S_{\tilde{w}_{\delta t_s, m}} \frac{T^3}{3} & S_{\tilde{w}_{\delta t_s, m}} \frac{T^2}{2} \\ S_{\tilde{w}_{\delta t_s, m}} \frac{T^2}{2} & S_{\tilde{w}_{\delta t_s, m}} T \end{bmatrix}.$$

The terms $S_{\tilde{w}_{\delta t_s, m}}$ and $S_{\tilde{w}_{\delta t_s, m}}$ are the clock bias and drift process noise power spectra, respectively, which can be related to the power-law coefficients, $\{h_{\alpha, s_m}\}_{\alpha=-2}^2$, which have been shown through laboratory experiments to characterize the power spectral density of the fractional frequency deviation of an oscillator from nominal frequency according to $S_{\tilde{w}_{\delta t_s, m}} \approx \frac{h_{0, s_m}}{2}$ and $S_{\tilde{w}_{\delta t_s, m}} \approx 2\pi^2 h_{-2, s_m}$ [28].

B. Receiver Dynamics Model

The receiver's planar position $\mathbf{r}_r \triangleq [x_r, y_r]^T$ and velocity $\dot{\mathbf{r}}_r$ will be assumed to evolve according to an arbitrary, but known, continuous-time dynamics model $\tilde{\mathbf{f}}_{\text{pv}}$ (e.g., velocity random walk or constant turn rate [29]). The receiver's state vector \mathbf{x}_r is defined by augmenting the receiver's position and velocity states $\mathbf{x}_{\text{pv}} \triangleq [\mathbf{r}_r^T, \dot{\mathbf{r}}_r^T]^T$ with its clock error states, $\mathbf{x}_{\text{clk}, r} \triangleq c[\delta t_r, \delta \dot{t}_r]^T$, i.e., $\mathbf{x}_r \triangleq [\mathbf{x}_{\text{pv}}^T, \mathbf{x}_{\text{clk}, r}^T]^T$. Discretizing the receiver's dynamics at a constant sampling period T yields

$$\begin{aligned} \mathbf{x}_r(k+1) &= \mathbf{f}_r[\mathbf{x}_r(k)] + \mathbf{w}_r(k), \\ \mathbf{f}_r[\mathbf{x}_r(k)] &\triangleq [\mathbf{f}_{\text{pv}}^T[\mathbf{x}_{\text{pv}}(k)], [\mathbf{F}_{\text{clk}} \mathbf{x}_{\text{clk}, r}(k)]^T]^T, \end{aligned}$$

where \mathbf{f}_{pv} is a vector-valued function, which is obtained by discretizing $\tilde{\mathbf{f}}_{\text{pv}}$ at a constant sampling interval T , \mathbf{w}_r is the process noise vector, which is modeled as a DT zero-mean white noise sequence with covariance $\mathbf{Q}_r = \text{diag}[\mathbf{Q}_{\text{pv}}, c^2 \mathbf{Q}_{\text{clk}, r}]$, where \mathbf{Q}_{pv} is the position and velocity process noise covariance and $\mathbf{Q}_{\text{clk}, r}$ is identical to $\mathbf{Q}_{\text{clk}, s_m}$, except that $S_{\tilde{w}_{\delta t_s, m}}$ and $S_{\tilde{w}_{\delta t_s, m}}$ are now replaced with receiver-specific spectra, $S_{\tilde{w}_{\delta t_r}}$ and $S_{\tilde{w}_{\delta \dot{t}_r}}$, respectively. A summary of the receiver and RF transmitter states are tabulated in Table I.

C. Measurement Model

The pseudorange measurement made by the receiver on the m^{th} RF transmitter, after discretization and mild approximations discussed in [19], is related to the receiver's and RF transmitter's states by

$$z_{s_m}(k) = \|\mathbf{r}_r(k) - \mathbf{r}_{s_m}\| + c \cdot [\delta t_r(k) - \delta t_{s_m}(k)] + v_{s_m}(k), \quad (1)$$

where $\|\cdot\|$ is the Euclidean norm and v_{s_m} is the measurement noise, which is modeled as a DT zero-mean white Gaussian sequence with variance $\sigma_{s_m}^2$.

D. Augmented System

The augmented system of an environment comprising one receiver and M RF transmitters will be denoted Σ and is given by

TABLE I
Receiver and RF Transmitter States

| States | Position | Velocity | Clock bias | Clock drift |
|--------------------|--------------------|----------------------|------------------|------------------------|
| Receiver | \mathbf{r}_r | $\dot{\mathbf{r}}_r$ | δt_r | $\delta \dot{t}_r$ |
| RF Transmitter m | \mathbf{r}_{s_m} | - | δt_{s_m} | $\delta \dot{t}_{s_m}$ |

$$\Sigma : \begin{cases} \mathbf{x}(k+1) = \mathbf{f}[\mathbf{x}(k)] + \mathbf{w}(k) \\ \mathbf{z}(k) = \mathbf{h}[\mathbf{x}(k)] + \mathbf{v}(k) \end{cases} \quad (2)$$

where $\mathbf{f}[\mathbf{x}(k)] \triangleq [\mathbf{f}_r^T[\mathbf{x}_r(k)], [\Phi_s \mathbf{x}_s(k)]^T]^T$; $\mathbf{x} \triangleq [\mathbf{x}_r^T, \mathbf{x}_s^T]^T$; $\Phi_s \triangleq \text{diag}[\mathbf{F}_s, \dots, \mathbf{F}_s]$; $\mathbf{x}_s = [\mathbf{x}_{s_1}^T, \dots, \mathbf{x}_{s_M}^T]^T$; $\mathbf{w} \triangleq [\mathbf{w}_r^T, \mathbf{w}_{s_1}^T, \dots, \mathbf{w}_{s_M}^T]^T$; $\mathbf{z} \triangleq [z_{s_1}, \dots, z_{s_M}]^T$; and $\mathbf{v} \triangleq [v_{s_1}, \dots, v_{s_M}]^T$, with covariance $\text{cov}(\mathbf{v}) \triangleq \mathbf{R} = \text{diag}[\sigma_{s_1}, \dots, \sigma_{s_M}]$.

III. STOCHASTIC OBSERVABILITY ANALYSIS

In this section, an overview of the EKF-based radio SLAM problem is presented, and the system's stochastic observability is studied according to the definition [21]:

DEFINITION III.1 A dynamic system is stochastically observable if and only if there exists a time t_b such that the estimation error covariance $\mathbf{P}_{\xi}(k|k)$ of the state vector ξ produced by a dynamic estimator remains upper bounded by σ_b in the sense that

$$\sigma_{\max}\{\mathbf{P}_{\xi}(k|k)\} \leq \sigma_b < \infty, \quad \forall kT \geq t_b,$$

where $\sigma_{\max}\{\mathbf{A}\}$ denotes the maximum singular value of \mathbf{A} .

A. EKF-Based Radio SLAM Overview

The goal of radio SLAM is for a receiver to construct and continuously refine a spatiotemporal signal landscape map of the environment, within which the receiver localizes itself in space and time. In the event that GNSS signals become unavailable or untrustworthy, the receiver continues navigating with the aid of this map. In EKF-based radio SLAM, an EKF produces an estimate $\hat{\mathbf{x}}(k|k) \triangleq \mathbb{E}[\mathbf{x}(k)|\mathbf{Z}^k]$ of $\mathbf{x}(k)$, where $\mathbb{E}[\cdot|\cdot]$ is the conditional expectation and \mathbf{Z}^k denotes all the measurements up to and including time-step k , i.e., $\mathbf{Z}^k \triangleq \{\mathbf{z}(j)\}_{j=1}^k$. In this paper, it is assumed that the receiver's initial state vector $\mathbf{x}_r(0)$ is known, which could be obtained from the last instant a reliable GNSS solution was available. The EKF-based radio SLAM prediction (time update) and correction (measurement update) are given by

1) *Prediction:*

$$\begin{aligned} \hat{\mathbf{x}}(k+1|k) &= \mathbf{F}(k)\hat{\mathbf{x}}(k|k), \\ \mathbf{P}_x(k+1|k) &= \mathbf{F}(k)\mathbf{P}_x(k|k)\mathbf{F}^T(k) + \mathbf{Q}. \end{aligned}$$

2) *Correction:*

$$\begin{aligned} \hat{\mathbf{x}}(k+1|k+1) &= \hat{\mathbf{x}}(k+1|k) + \mathbf{L}(k+1)\mathbf{S}^{-1}\mathbf{v}(k+1), \\ \mathbf{P}_x(k+1|k+1) &= \mathbf{P}_x(k+1|k) - \mathbf{L}(k+1)\mathbf{S}^{-1}(k+1) \\ &\quad \times \mathbf{L}^T(k+1), \end{aligned}$$

where $\hat{\mathbf{x}}(k+1|k)$ and $\hat{\mathbf{x}}(k+1|k+1)$ are the predicted and corrected state estimates, respectively; $\mathbf{P}_x(k+1|k)$

and $\mathbf{P}_x(k+1|k+1)$ are the prediction error covariance and corrected estimation error covariance, respectively; \mathbf{F} is the Jacobian of \mathbf{f} evaluated at the current state estimate $\hat{\mathbf{x}}(k|k)$; $\mathbf{v}(k+1) \triangleq \mathbf{z}(k+1) - \hat{\mathbf{z}}(k+1|k)$ is the innovation; $\hat{\mathbf{z}}(k+1|k) \triangleq \mathbf{h}[\hat{\mathbf{x}}(k+1|k)]$ is the measurement prediction; $\mathbf{L}(k+1) \triangleq \mathbf{P}_x(k+1|k)\mathbf{H}^\top(k+1)$; $\mathbf{S}(k+1) \triangleq \mathbf{H}(k+1)\mathbf{L}(k+1) + \mathbf{R}$ is the innovation covariance; and $\mathbf{H}(k+1)$ is the Jacobian of \mathbf{h} evaluated at $\hat{\mathbf{x}}(k+1|k)$, which has the form

$$\mathbf{H} = \begin{bmatrix} \mathbf{h}_{r,s_1}^\top & \mathbf{h}_{s_1}^\top & \cdots & \mathbf{0}_{1 \times 4} \\ \vdots & \vdots & \ddots & \vdots \\ \mathbf{h}_{r,s_M}^\top & \mathbf{0}_{1 \times 4} & \cdots & \mathbf{h}_{s_M}^\top \end{bmatrix},$$

$$\mathbf{h}_{r,s_m}^\top(k) = \begin{bmatrix} \hat{\mathbf{1}}_m^\top(k), & \mathbf{0}_{1 \times 2}, & \mathbf{h}_{\text{clk}}^\top \end{bmatrix},$$

$$\mathbf{h}_{s_m}^\top(k) = \begin{bmatrix} -\hat{\mathbf{1}}_m^\top(k), & -\mathbf{h}_{\text{clk}}^\top \end{bmatrix}, \quad \mathbf{h}_{\text{clk}} = \begin{bmatrix} 1 \\ 0 \end{bmatrix},$$

$$\hat{\mathbf{1}}_m(k) \triangleq \frac{\hat{\mathbf{r}}_r(k|k-1) - \hat{\mathbf{r}}_{s_m}(k|k-1)}{\|\hat{\mathbf{r}}_r(k|k-1) - \hat{\mathbf{r}}_{s_m}(k|k-1)\|},$$

$$m = 1, \dots, M.$$

B. Stochastically Unobservable Clock Errors

This section shows that the EKF estimating the state vector of the system in (2) produces an estimation error covariance matrix $\mathbf{P}_x(k|k)$ whose time evolution grows unboundedly.

Traditional deterministic observability tests provide a necessary, but not sufficient condition for stochastic observability [21]. They also do not incorporate *a priori* knowledge of the uncertainty about the initial state estimate $\mathbf{P}_x(0|0)$, process noise covariance \mathbf{Q} , or measurement noise covariance \mathbf{R} . Moreover, since they only provide a Boolean assessment of the observability of a system, if the system is stochastically unobservable, they do not yield any characterization or the rate of divergence of unobservable states. In what follows, the time evolution of the Riccati equation is studied to show that the radio SLAM problem is stochastically unobservable and to derive a lower bound for the rate of divergence of stochastically unobservable states.

LEMMA III.1 If the estimation error covariance matrix $\mathbf{P}_\xi(k|k)$ is such that

$$\lim_{k \rightarrow \infty} \mathbf{e}_i^\top \mathbf{P}_\xi(k|k) \mathbf{e}_i = \infty, \quad (3)$$

where \mathbf{e}_i denotes the i th standard basis vector consisting of a 1 in the i th element and zeros elsewhere, then the i th state of $\xi \in \mathbb{R}^n$ is stochastically unobservable, and subsequently the system is stochastically unobservable.

PROOF If $\lim_{k \rightarrow \infty} \mathbf{e}_i^\top \mathbf{P}_\xi(k|k) \mathbf{e}_i = \infty$, then

$$\lim_{k \rightarrow \infty} \text{tr}[\mathbf{P}_\xi(k|k)] = \lim_{k \rightarrow \infty} \sum_{i=1}^n \mathbf{e}_i^\top \mathbf{P}_\xi(k|k) \mathbf{e}_i = \infty,$$

where $\text{tr}[\mathbf{A}]$ denotes the trace of \mathbf{A} . From the trace properties, $\text{tr}[\mathbf{P}_\xi(k|k)] = \sum_{i=1}^n \lambda_i[\mathbf{P}_\xi(k|k)]$, where $\lambda_i[\mathbf{A}]$ de-

notes the i th eigenvalue of \mathbf{A} . Since $\mathbf{P}_\xi(k|k)$ is symmetric positive semidefinite, its singular values $\sigma_i[\mathbf{P}_\xi(k|k)] = \lambda_i[\mathbf{P}_\xi(k|k)]$. Therefore

$$\begin{aligned} \lim_{k \rightarrow \infty} \text{tr}[\mathbf{P}_\xi(k|k)] &= \lim_{k \rightarrow \infty} \sum_{i=1}^n \lambda_i[\mathbf{P}_\xi(k|k)] \\ &= \lim_{k \rightarrow \infty} \sum_{i=1}^n \sigma_i[\mathbf{P}_\xi(k|k)] = \infty. \end{aligned}$$

Since n is finite, then at least the largest singular value will grow unboundedly, i.e., $\lim_{k \rightarrow \infty} \sigma_{\max}[\mathbf{P}_\xi(k|k)] = \infty$, where $\sigma_{\max}[\mathbf{A}] = \max_i \{\sigma_i[\mathbf{A}]\}$, making the system stochastically unobservable. ■

THEOREM III.1 The radio SLAM problem consisting of one receiver with knowledge of its initial states and M unknown RF transmitters is stochastically unobservable regardless of the receiver's motion. Moreover, δt_r and $\{\delta t_{s_m}\}_{m=1}^M$ are stochastically unobservable states.

PROOF The proof will proceed in two main steps. First, three simplified systems will be defined, denoted Σ_I , Σ_{II} , and Σ_{III} , where Σ_I is a simplified form of Σ and each subsequent system is a simplified version of the preceding one. It is shown that if the subsequent system is stochastically unobservable, then the preceding system must be stochastically unobservable as well. Second, Σ_{III} is shown to be stochastically unobservable according to Definition III.1 by invoking lemma III.1.

Step 1: First, define Σ_I as a system with 1) known RF transmitter position states $\{\mathbf{r}_{s_m}\}_{m=1}^M$ and 2) no process noise driving the receiver's position and velocity states (i.e., $\mathbf{Q}_{\text{pv}} = \mathbf{0}$), e.g., a receiver moving with a constant velocity. From 1) and 2), and since $\mathbf{r}_r(0)$ is known, it is obvious that $\{\mathbf{r}_{s_m}\}_{m=1}^M$ and $\mathbf{r}_r(k)$ are known $\forall k$ and need not be estimated by the EKF, simplifying the system to be estimated to a linear time-invariant (LTI) system, given by

$$\Sigma_I : \begin{cases} \mathbf{x}_{\text{clk}}(k+1) = \Phi_{\text{clk}} \mathbf{x}_{\text{clk}}(k) + \mathbf{w}_{\text{clk}}(k) \\ \mathbf{z}_{\text{clk}}(k) = \mathbf{H}_{\text{clk}} \mathbf{x}_{\text{clk}}(k) + \mathbf{v}(k), \end{cases}$$

where

$$\begin{aligned} \mathbf{x}_{\text{clk}} &\triangleq [\mathbf{x}_{\text{clk},r}^\top, \mathbf{x}_{\text{clk},s_1}^\top, \dots, \mathbf{x}_{\text{clk},s_M}^\top]^\top \in \mathbb{R}^{(2+2M)}, \\ \Phi_{\text{clk}} &\triangleq \text{diag}[\mathbf{F}_{\text{clk}}, \dots, \mathbf{F}_{\text{clk}}] \in \mathbb{R}^{[(2+2M) \times (2+2M)]}, \\ \mathbf{z}_{\text{clk}} &\triangleq [\mathbf{z}_{\text{clk},s_1}, \dots, \mathbf{z}_{\text{clk},s_M}]^\top, \\ \mathbf{H}_{\text{clk}} &= \begin{bmatrix} \mathbf{h}_{\text{clk}}^\top & -\mathbf{h}_{\text{clk}}^\top & \cdots & \mathbf{0}_{1 \times 2} \\ \vdots & \vdots & \ddots & \vdots \\ \mathbf{h}_{\text{clk}}^\top & \mathbf{0}_{1 \times 2} & \cdots & -\mathbf{h}_{\text{clk}}^\top \end{bmatrix}, \end{aligned}$$

where \mathbf{w}_{clk} is a DT zero-mean white process noise vector with covariance $\mathbf{Q}_{\text{clk}} = c^2 \cdot \text{diag}[\mathbf{Q}_{\text{clk},r}, \mathbf{Q}_{\text{clk},s_1}, \dots, \mathbf{Q}_{\text{clk},s_M}]$. The measurements have the form $\mathbf{z}_{\text{clk},s_m}(k) \triangleq z_m(k) - \|\mathbf{r}_r(k) - \mathbf{r}_{s_m}\|$ for $m = 1, \dots, M$.

Since system Σ_I is LTI, a Kalman filter (KF) may be employed to estimate the state vector \mathbf{x}_{clk} . To incorporate perfect *a priori* knowledge of $\mathbf{x}_{\text{clk},r}(0)$ in the KF, the corresponding block of the initial estimation error covariance matrix is set to zero. Assuming the initial estimates of $\{\mathbf{x}_{\text{clk},s_m}\}_{m=1}^M$ to be uncorrelated, the initial estimation error covariance matrix is given as follows:

$${}^I\mathbf{P}_{\mathbf{x}_{\text{clk}}}(0|0) = \text{diag}[\mathbf{0}_{2 \times 2}, {}^I\mathbf{P}_{\mathbf{x}_{\text{clk},s}}(0|0)], \quad (4)$$

where ${}^I\mathbf{P}_{\mathbf{x}_{\text{clk}}}(0|0)$ is the initial estimation error covariance of the KF associated with Σ_I

$${}^I\mathbf{P}_{\mathbf{x}_{\text{clk},s}}(0|0) \triangleq \text{diag}\left[{}^I\sigma_{\delta t_{s_1}}^2(0|0), {}^I\sigma_{\delta t_{s_1}}^2(0|0), \dots, {}^I\sigma_{\delta t_{s_M}}^2(0|0), {}^I\sigma_{\delta t_{s_M}}^2(0|0)\right],$$

is the initial estimation error covariance of the state vectors $\{\mathbf{x}_{\text{clk},s_m}\}_{m=1}^M$, and ${}^I\sigma_{\delta t_{s_m}}^2$ and ${}^I\sigma_{\delta t_{s_m}}^2$ are the variances of the transmitters' clock bias and drift, respectively.

Define Σ_{II} to be the same as Σ_I with the additional simplifications that $S_{\tilde{w}_{\delta t_r}} = 0$ and $\{S_{\tilde{w}_{\delta t_{s_m}}}\}_{m=1}^M = 0$. Since Σ_{II} has less process noise than Σ_I , it is obvious that ${}^{II}\mathbf{P}_{\mathbf{x}_{\text{clk}}}(k+1|k) < {}^I\mathbf{P}_{\mathbf{x}_{\text{clk}}}(k+1|k)$, $\forall k$, where $\mathbf{A} < \mathbf{B}$ denotes the difference $\mathbf{B} - \mathbf{A}$ being positive definite. Therefore, if Σ_{II} is stochastically unobservable, then Σ_I must be stochastically unobservable as well.

Define Σ_{III} to be the same as Σ_{II} with the additional simplification that $\mathbf{R} = \mathbf{0}_{M \times M}$. Since Σ_{III} has no measurement noise, it is obvious that ${}^{III}\mathbf{P}_{\mathbf{x}_{\text{clk}}}(k+1|k+1) < {}^{II}\mathbf{P}_{\mathbf{x}_{\text{clk}}}(k+1|k+1)$, $\forall k$. Therefore, if Σ_{III} is stochastically unobservable, then Σ_{II} must be stochastically unobservable as well. Also, since for each k there are M perfect measurements that are linearly related to $2 + 2M$ states, the state vector order of Σ_{III} may be reduced from $2 + 2M$ to $2 + M$ and a reduced-order KF may be used. Reduced-order KFs are used in practice to avoid potential numerical issues and reduce computational complexity [30]. It turns out that the reduced-order KF lends itself to a tractable closed-form expression of the time evolution of the associated estimation error covariance; therefore, is used to evaluate the stochastic observability of Σ_{III} for the second part of this proof.

Step 2: An estimate of $\mathbf{x}_{\text{clk}}(k)$ can be computed though

$$\hat{\mathbf{x}}_{\text{clk}}(k|k) = \mathbf{L}_1 \mathbf{z}_{\text{clk}}(k) + \mathbf{L}_2 \hat{\mathbf{x}}_{\text{ro}}(k|k), \quad (5)$$

where $\hat{\mathbf{x}}_{\text{ro}}(k|k)$ is an estimate produced by a reduced-order KF of the reduced-order state vector $\mathbf{x}_{\text{ro}}(k) \triangleq \mathbf{G}\mathbf{x}_{\text{clk}}(k)$; $(\mathbf{L}_1|\mathbf{L}_2) \triangleq (\frac{\mathbf{H}_{\text{clk}}}{\mathbf{G}})^{-1}$; $(\mathbf{L}_1|\mathbf{L}_2)$ is the matrix formed by augmenting the columns of \mathbf{L}_1 and \mathbf{L}_2 ; $(\frac{\mathbf{H}_{\text{clk}}}{\mathbf{G}})$ is the matrix formed by augmenting the rows of \mathbf{H}_{clk} and \mathbf{G} ; and \mathbf{G} is the design matrix which is chosen to be

$$\mathbf{G} \equiv \begin{bmatrix} \mathbf{I}_2 & \mathbf{0}_{2 \times 2} & \dots & \mathbf{0}_{2 \times 2} \\ \mathbf{g}^\top & -\mathbf{g}^\top & \dots & \mathbf{0}_{1 \times 2} \\ \vdots & \vdots & \ddots & \vdots \\ \mathbf{g}^\top & \mathbf{0}_{1 \times 2} & \dots & -\mathbf{g}^\top \end{bmatrix}, \quad \mathbf{g} \triangleq \begin{bmatrix} 0 \\ 1 \end{bmatrix}, \quad (6)$$

so that δt_r is the first state of \mathbf{x}_{ro} and $(\frac{\mathbf{H}_{\text{clk}}}{\mathbf{G}})$ is invertible. It is important to note that although the choice of \mathbf{G} and the corresponding reduced-order state vector \mathbf{x}_{ro} are nonunique, the remainder of the proof is invariant to any feasible choice of \mathbf{G} that makes $(\frac{\mathbf{H}_{\text{clk}}}{\mathbf{G}})$ invertible.

A reduced-order KF produces $\hat{\mathbf{x}}_{\text{ro}}(k+1|k+1)$ and an associated posterior estimation error covariance given by

$$\begin{aligned} \mathbf{P}_{\mathbf{x}_{\text{ro}}}(k+1|k+1) &= [\Psi - \Lambda(k)\Xi] \mathbf{P}_{\mathbf{x}_{\text{ro}}}(k|k) [\Psi - \Lambda(k)\Xi]^\top \\ &\quad + \mathbf{G}\mathbf{Q}_{\text{clk}}\mathbf{G}^\top - \mathbf{G}\mathbf{Q}_{\text{clk}}\mathbf{H}_{\text{clk}}^\top \Lambda^\top(k) \\ &\quad - \Lambda(k)\mathbf{H}_{\text{clk}}\mathbf{Q}_{\text{clk}}^\top \mathbf{G}^\top + \Lambda(k)\mathbf{R}_{\text{ro}}\Lambda^\top(k), \end{aligned} \quad (7)$$

where $\Psi \triangleq \mathbf{G}\Phi_{\text{clk}}\mathbf{L}_2$, $\Xi \triangleq \mathbf{H}_{\text{clk}}\Phi_{\text{clk}}\mathbf{L}_2$, $\mathbf{R}_{\text{ro}} \triangleq \mathbf{H}_{\text{clk}}\mathbf{Q}_{\text{clk}}\mathbf{H}_{\text{clk}}^\top$, and

$$\begin{aligned} \Lambda(k) &= [\Psi \mathbf{P}_{\mathbf{x}_{\text{ro}}}(k|k) \Xi^\top + \mathbf{G}\mathbf{Q}_{\text{clk}}\mathbf{H}_{\text{clk}}^\top] \\ &\quad \cdot [\Xi \mathbf{P}_{\mathbf{x}_{\text{ro}}}(k|k) \Xi^\top + \mathbf{R}_{\text{ro}}]^{-1}. \end{aligned} \quad (8)$$

Note that the matrix $\Xi \mathbf{P}_{\mathbf{x}_{\text{ro}}}(k|k) \Xi^\top$ is symmetric positive semidefinite $\forall k$ and \mathbf{R}_{ro} is symmetric positive definite and time-invariant; therefore, $[\Xi \mathbf{P}_{\mathbf{x}_{\text{ro}}}(k|k) \Xi^\top + \mathbf{R}_{\text{ro}}]$ is symmetric positive definite and invertible $\forall k$.

The estimate of $\hat{\mathbf{x}}_{\text{clk}}(k+1|k+1)$ is then produced through (5) and its corresponding posterior estimation error covariance is

$${}^{III}\mathbf{P}_{\mathbf{x}_{\text{clk}}}(k+1|k+1) = \mathbf{L}_2 \mathbf{P}_{\mathbf{x}_{\text{ro}}}(k+1|k+1) \mathbf{L}_2^\top, \quad (9)$$

where $\mathbf{L}_2 = [\mathbf{e}_1, \mathbf{e}_2, \mathbf{e}_1, \mathbf{e}_2 - \mathbf{e}_3, \dots, \mathbf{e}_1, \mathbf{e}_2 - \mathbf{e}_{M+2}]^\top$. From (9) and the structure of \mathbf{L}_2 , the clock bias estimation error variances of the receiver and the RF transmitters are equal, i.e.,

$${}^{III}\sigma_{\delta t_r}^2(k|k) = \{{}^{III}\sigma_{\delta t_{s_m}}^2(k|k)\}_{m=1}^M. \quad (10)$$

This equality holds for any feasible \mathbf{G} , since there are M perfect measurements; therefore, the biases of the receiver and RF transmitters are linearly related to each other by a deterministic quantity, given by $\delta t_r = \delta t_{s_m} + z_{\text{clk},s_m}$, for $m = 1, \dots, M$. A closed-form expression of the time evolution of ${}^{III}\sigma_{\delta t_r}^2(k|k)$ is found through the following two steps. First, (7) is recursively solved using an initial estimation error covariance given by

$$\mathbf{P}_{\mathbf{x}_{\text{ro}}}(0|0) = \mathbf{G} {}^{III}\mathbf{P}_{\mathbf{x}_{\text{clk}}}(0|0) \mathbf{G}^\top,$$

where ${}^{III}\mathbf{P}_{\mathbf{x}_{\text{clk}}}(0|0)$ has the same structure as (4), except \mathbf{I} is replaced with \mathbf{III} . Second, the element corresponding to the receiver's clock bias $\mathbf{e}_1^\top {}^{III}\mathbf{P}_{\mathbf{x}_{\text{clk}}}(k|k) \mathbf{e}_1$ is found by substituting the right-hand side of (7) into (9), yielding

$${}^{III}\sigma_{\delta t_r}^2(k|k) = \frac{kq_r \prod_{m=1}^M \Omega_m(k)}{\det[k\Xi \mathbf{P}_{\mathbf{x}_{\text{ro}}}(0|0) \Xi^\top + \mathbf{R}_{\text{ro}}]}, \quad k = 1, 2, \dots, \quad (11)$$

where $\Omega_m(k) \triangleq q_{s_m} + kT^2\beta_m$, $\beta_m = {}^{III}\sigma_{\delta t_{s_m}}^2(0|0)$, $q_r \triangleq c^2 S_{\tilde{w}_{\delta t_r}} T$, and $q_{s_m} \triangleq c^2 S_{\tilde{w}_{\delta t_{s_m}}} T$. Finally, to evaluate the limit (3) for the first state of ${}^{III}\mathbf{P}_{\mathbf{x}_{\text{clk}}}$, the closed-form (11) is used,

yielding

$$\begin{aligned}
& \lim_{k \rightarrow \infty} \mathbf{e}_1^\top \mathbf{P}_{\mathbf{x}_{\text{clk}}}^{\text{III}}(k|k) \mathbf{e}_1 \\
&= \lim_{k \rightarrow \infty} {}^{\text{III}}\sigma_{\delta_{t_r}}^2(k|k) \\
&= \lim_{k \rightarrow \infty} \frac{k q_r \prod_{m=1}^M \Omega_m(k)}{\det[k \Xi \mathbf{P}_{\mathbf{x}_{\text{ro}}}(0|0) \Xi^\top + \mathbf{R}_{\text{ro}}]} \\
&= \lim_{k \rightarrow \infty} \frac{k^{(M+1)} q_r \prod_{m=1}^M (\frac{1}{k} q_{s_m} + T^2 \beta_m)}{k^M \det[\Xi \mathbf{P}_{\mathbf{x}_{\text{ro}}}(0|0) \Xi^\top + \frac{1}{k} \mathbf{R}_{\text{ro}}]} = \infty. \quad (12)
\end{aligned}$$

Therefore, stochastic unobservability follows from Lemma III.1. ■

THEOREM III.2 The EKF estimating the receiver's state simultaneously with the states of M terrestrial transmitters, with a priori knowledge about the receiver's initial state, for the stochastically unobservable system Σ , produces corresponding estimation error variances $\sigma_{\delta_{t_r}}^2$ and $\{\sigma_{\delta_{t_{s_m}}}^2\}_{m=1}^M$, respectively, whose time evolution is lower-bounded by a diverging sequence with a divergence rate $\gamma(k)$, where $\gamma(k) \xrightarrow{k \rightarrow \infty} c^2 S_{\tilde{w}_{\delta_{t_r}}} T$.

PROOF From Theorem III.1, system Σ is stochastically unobservable and the variances $\sigma_{\delta_{t_r}}^2$ and $\{\sigma_{\delta_{t_{s_m}}}^2\}_{m=1}^M$ produced by an EKF will diverge and their time evolutions are lower bounded by (11).

Define the divergence rate of the estimation error variance associated with the i th state of the vector $\xi \in \mathbb{R}^n$ as follows:

$$\gamma(k) = \mathbf{e}_i^\top [\mathbf{U}_{\xi, \text{inc}}(k) - \mathbf{U}_{\xi, \text{red}}(k)] \mathbf{e}_i, \quad (13)$$

where

$$\mathbf{U}_{\xi, \text{inc}}(k) \triangleq \mathbf{P}_{\xi}(k+1|k) - \mathbf{P}_{\xi}(k|k)$$

is the uncertainty increase from the EKF prediction step and

$$\mathbf{U}_{\xi, \text{red}}(k) \triangleq \mathbf{P}_{\xi}(k+1|k) - \mathbf{P}_{\xi}(k+1|k+1)$$

is the uncertainty reduction from the EKF correction step.

Substituting (11) into (13) for the first state of ${}^{\text{III}}\mathbf{P}_{\mathbf{x}_{\text{clk}}}$ gives

$$\begin{aligned}
& \mathbf{e}_1^\top [\mathbf{U}_{\mathbf{x}_{\text{clk}}, \text{inc}}(k) - \mathbf{U}_{\mathbf{x}_{\text{clk}}, \text{red}}(k)] \mathbf{e}_1 \\
&= {}^{\text{III}}\sigma_{\delta_{t_r}}^2(k+1|k+1) - {}^{\text{III}}\sigma_{\delta_{t_r}}^2(k|k) \\
&= \frac{(k+1) q_r \prod_{m=1}^M \Omega_m(k+1)}{\det[(k+1) \Xi \mathbf{P}_{\mathbf{x}_{\text{ro}}}(0|0) \Xi^\top + \mathbf{R}_{\text{ro}}]} \\
&\quad - \frac{k q_r \prod_{m=1}^M \Omega_m(k)}{\det[k \Xi \mathbf{P}_{\mathbf{x}_{\text{ro}}}(0|0) \Xi^\top + \mathbf{R}_{\text{ro}}]}. \quad (14)
\end{aligned}$$

Evaluating the limit of (14) yields

$$\begin{aligned}
& \lim_{k \rightarrow \infty} \mathbf{e}_1^\top [\mathbf{U}_{\mathbf{x}_{\text{clk}}, \text{inc}}(k) - \mathbf{U}_{\mathbf{x}_{\text{clk}}, \text{red}}(k)] \mathbf{e}_1 \\
&= \lim_{k \rightarrow \infty} \frac{[k+1]^{(M+1)} q_r \prod_{m=1}^M (\frac{1}{k+1} q_{s_m} + T^2 \beta_m)}{[k+1]^M \det[\Xi \mathbf{P}_{\mathbf{x}_{\text{ro}}}(0|0) \Xi^\top + \frac{1}{k+1} \mathbf{R}_{\text{ro}}]} \\
&\quad - \lim_{k \rightarrow \infty} \frac{k^{(M+1)} q_r \prod_{m=1}^M (\frac{1}{k} q_{s_m} + T^2 \beta_m)}{k^M \det[\Xi \mathbf{P}_{\mathbf{x}_{\text{ro}}}(0|0) \Xi^\top + \frac{1}{k} \mathbf{R}_{\text{ro}}]} \\
&= \frac{q_r \lim_{k \rightarrow \infty} (k+1) \prod_{m=1}^M (T^2 \beta_m)}{\det[\Xi \mathbf{P}_{\mathbf{x}_{\text{ro}}}(0|0) \Xi^\top]} \\
&\quad - \frac{q_r \lim_{k \rightarrow \infty} k \prod_{m=1}^M (T^2 \beta_m)}{\det[\Xi \mathbf{P}_{\mathbf{x}_{\text{ro}}}(0|0) \Xi^\top]} \\
&= \frac{q_r \prod_{m=1}^M (T^2 \beta_m)}{\prod_{m=1}^M (T^2 \beta_m)} = q_r, \quad (15)
\end{aligned}$$

where $q_r \triangleq c^2 S_{\tilde{w}_{\delta_{t_r}}} T$. ■

Theorem III.1 shows that the radio SLAM problem with *a priori* knowledge about the receiver's states is stochastically unobservable, since the estimation uncertainty associated with the clock biases of both the receivers and terrestrial transmitters will diverge. Theorem III.2 establishes a lower bound of this divergence, which in the limit, only depends on the quality of the receiver's clock, characterized by $S_{\tilde{w}_{\delta_{t_r}}}$. The following two sections present numerical and experimental results demonstrating radio SLAM.

IV. SIMULATION RESULTS

In this section, an environment consisting of one UAV-mounted receiver and $M = 5$ RF transmitters is simulated to demonstrate that both the receiver's clock bias δ_{t_r} and the transmitters' clock biases $\{\delta_{t_{s_m}}\}_{m=1}^M$ are stochastically unobservable, as was shown in Theorem III.1 and to demonstrate that the divergence rate $\gamma(k) \xrightarrow{k \rightarrow \infty} q_r$, as established in Theorem III.2. To this end, two systems are simulated: 1) system Σ_{III} to demonstrate the divergence rate $\gamma(k) \xrightarrow{k \rightarrow \infty} q_r$ (15) and 2) the full system Σ to demonstrate the divergence of the estimation error variances of the clock biases when the receiver's position and velocity and the transmitters' positions are also estimated.

First, an estimate $\hat{\mathbf{x}}_{\text{clk}}(k|k)$ of Σ_{III} 's state vector was computed through (5), using the design matrix (6) and the estimate $\hat{\mathbf{x}}_{\text{ro}}(k|k)$, which was produced by a reduced-order KF. The reduced-order KF was initialized according to $\hat{\mathbf{x}}_{\text{ro}}(0|0) \sim \mathcal{N}[\mathbf{G} \mathbf{x}_{\text{clk}}(0), \mathbf{P}_{\mathbf{x}_{\text{ro}}}(0|0)]$, where $\mathbf{P}_{\mathbf{x}_{\text{ro}}}(0|0) = \mathbf{G} [{}^{\text{III}}\mathbf{P}_{\mathbf{x}_{\text{clk}}}(0|0)] \mathbf{G}^\top$. The simulation settings are tabulated in Table II. The nonzero estimation error trajectories $\tilde{\mathbf{x}}_{\text{ro}} \triangleq \mathbf{x}_{\text{ro}} - \hat{\mathbf{x}}_{\text{ro}}$ and their associated $\pm 2\sigma$ bounds are plotted in Fig. 1(a)–(b). The time evolution of $\gamma(k) = \mathbf{e}_1^\top [\mathbf{U}_{\mathbf{x}_{\text{ro}}, \text{inc}}(k) - \mathbf{U}_{\mathbf{x}_{\text{ro}}, \text{red}}(k)] \mathbf{e}_1$ is plotted in Fig. 1(c). The estimation error $\tilde{\mathbf{x}}_{\text{clk}} \triangleq \mathbf{x}_{\text{clk}} - \hat{\mathbf{x}}_{\text{clk}}$ was reconstructed from (5) and the associated posterior estimation error covariance ${}^{\text{III}}\mathbf{P}_{\mathbf{x}_{\text{clk}}}$ was computed by substituting the reduced-order KF's posterior estimation error covariance (7) into (9).

TABLE II
Simulation Settings: System Σ_{III}

| Parameter | Value |
|---|---|
| $\mathbf{x}_{\text{clk}_r}(0)$ | $[100, 10]^T$ |
| $\{\mathbf{x}_{\text{clk}_{s_m}}(0)\}_{m=1}^5$ | $[10, 1]^T$ |
| $\mathbf{x}_{\text{clk}}(0)$ | $[\mathbf{x}_{\text{clk}_r}^T(0), \mathbf{x}_{\text{clk}_{s_1}}^T(0), \dots, \mathbf{x}_{\text{clk}_{s_5}}^T(0)]^T$ |
| ${}^{III}\mathbf{P}_{\mathbf{x}_{\text{clk}}}(0 0)$ | $(10^2) \cdot \text{diag}[0, 0, 3, 0.3, \dots, 3, 0.3]$ |
| $\{h_{0,r}, h_{-2,r}\}$ | $\{9.4 \times 10^{-20}, 0\}$ |
| $\{h_{0,s_m}, h_{-2,s_m}\}_{m=1}^5$ | $\{8.0 \times 10^{-20}, 0\}$ |
| T | 0.01 s |
| $\{\sigma_{s_m}^2\}_{m=1}^5$ | 0 m ² |

The estimation error trajectories and corresponding $\pm 2\sigma$ bounds for δt_r , δt_{s_1} , and δt_{s_5} are plotted in Fig. 1(d)–(f).

The following can be concluded from these plots. First, ${}^{III}\sigma_{\delta t_r}^2(k|k) = {}^{III}\sigma_{\delta t_s}^2(k|k) \forall k$, as expected from (10). Second, ${}^{III}\sigma_{\delta t_r}^2$ and ${}^{III}\sigma_{\delta t_{s_1}}^2$ are diverging, implying δt_r and δt_{s_1} are stochastically unobservable. The same behavior was observed for the variances associated with $\{\delta t_{s_m}\}_{m=2}^5$. Third, Fig. 1(c) illustrates that their divergence rate converges to a constant, $\gamma(k) \xrightarrow{k \rightarrow \infty} q_r$, as established in Theorem III.2. The diverging errors were noted to be consistent with their $\pm 2\sigma$ bounds when the simulator was ran using different realizations of process noise and initial state estimates.

Next, the full system Σ was simulated and an EKF was employed to estimate $\mathbf{x}(k)$. The purpose of this simulation is to illustrate that δt_r and $\{\delta t_{s_m}\}_{m=1}^5$ are stochastically unobservable in the full system Σ and to demonstrate the behavior of the estimation errors of the receiver's position and velocity and the RF transmitters' positions, along with their corresponding variances. The receiver moved in a favorable trajectory around the RF transmitters. Specifically, the receiver's position and velocity states were set to evolve according to a constant turn rate model as described in [29], i.e., $\mathbf{f}_{\text{pv}}[\mathbf{x}_{\text{pv}}(k)]$ and \mathbf{Q}_{pv} were set to the equations shown

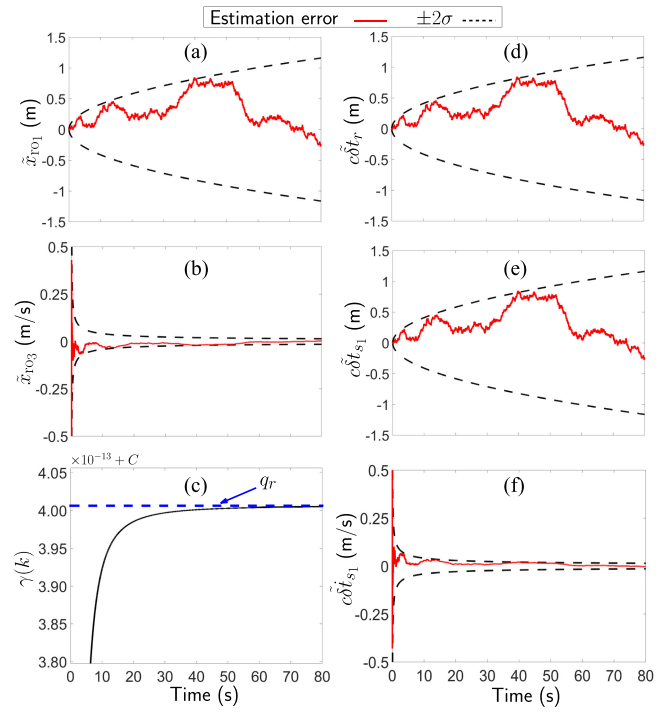


Fig. 1. Estimation error trajectories (red) and corresponding $\pm 2\sigma$ bounds (black dashed). (a) and (b) correspond to a reduced-order KF estimating \mathbf{x}_{ro} using settings from Table II, where $\mathbf{x}_{ro_i} \triangleq \mathbf{e}_i^T \mathbf{x}_{ro}$. (c) illustrates the time evolution of $\gamma(k) = \mathbf{e}_1^T [\mathbf{U}_{\mathbf{x}_{\text{clk}}, \text{inc}}(k) - \mathbf{U}_{\mathbf{x}_{\text{clk}}, \text{red}}(k)] \mathbf{e}_1$ (black) and the value of its limit q_r (blue dotted), where $C = 4.2241493 \times 10^{-5}$. (d)–(f) correspond to the clock errors of the receiver and transmitter 1, which were reconstructed through (5), and their corresponding $\pm 2\sigma$ bounds, which were computed using (7) and (9).

at the bottom of the page, where $\text{s}(\cdot)$ and $\text{c}(\cdot)$ denote $\sin(\cdot)$ and $\cos(\cdot)$, respectively, ω is a known constant turn rate, and S_w is the process noise power spectral density. This type of open-loop trajectory has been demonstrated to produce better estimates than an open-loop velocity random walk

$$\mathbf{f}_{\text{pv}}[\mathbf{x}_{\text{pv}}(k)] \equiv \begin{bmatrix} 1 & 0 & \frac{\text{s}(\omega T)}{\omega} & -\frac{1 - \text{c}(\omega T)}{\omega} \\ 0 & 1 & \frac{1 - \text{c}(\omega T)}{\omega} & \frac{\text{s}(\omega T)}{\omega} \\ 0 & 0 & \text{c}(\omega T) & -\text{s}(\omega T) \\ 0 & 0 & \text{s}(\omega T) & \text{c}(\omega T) \end{bmatrix} \mathbf{x}_{\text{pv}}(k)$$

$$\mathbf{Q}_{\text{pv}} \equiv S_w \begin{bmatrix} 2\frac{\omega T - \text{s}(\omega T)}{\omega^3} & 0 & \frac{1 - \text{c}(\omega T)}{\omega^2} & \frac{\omega T - \text{s}(\omega T)}{\omega^2} \\ 0 & 2\frac{\omega T - \text{s}(\omega T)}{\omega^3} & -\frac{\omega T - \text{s}(\omega T)}{\omega^2} & \frac{1 - \text{c}(\omega T)}{\omega^2} \\ \frac{1 - \text{c}(\omega T)}{\omega^2} & -\frac{\omega T - \text{s}(\omega T)}{\omega^2} & T & 0 \\ \frac{\omega T - \text{s}(\omega T)}{\omega^2} & \frac{1 - \text{c}(\omega T)}{\omega^2} & 0 & T \end{bmatrix}$$

TABLE III
Simulation Settings: System Σ

| Parameter | Value |
|-------------------------------------|--|
| $\mathbf{x}_r(0)$ | $[0, 0, 10, 10, 100, 10]^\top$ |
| $\mathbf{P}_r(0 0)$ | $\text{diag}[0, 0, 0, 0, 0, 0]$ |
| $\{h_{0,r}, h_{-2,r}\}$ | $\{9.4 \times 10^{-20}, 3.8 \times 10^{-21}\}$ |
| $\mathbf{r}_{s_1}(0)$ | $[-110, 240]^\top$ |
| $\mathbf{r}_{s_2}(0)$ | $[-150, 340]^\top$ |
| $\mathbf{r}_{s_3}(0)$ | $[-215, -60]^\top$ |
| $\mathbf{r}_{s_4}(0)$ | $[-75, 105]^\top$ |
| $\mathbf{r}_{s_5}(0)$ | $[-5, 80]^\top$ |
| $\mathbf{x}_{s_m}(0)$ | $[\mathbf{r}_{s_m}^\top, 10, 1]^\top$ |
| $\mathbf{P}_{s_m}(0 0)$ | $(10^2) \cdot \text{diag}[1, 1, 30, 3]$ |
| $\hat{\mathbf{x}}_{s_m}(0 0)$ | $\sim \mathcal{N}[\mathbf{x}_{s_m}(0), \mathbf{P}_{s_m}(0 0)]$ |
| $\{h_{0,s_m}, h_{-2,s_m}\}_{m=1}^5$ | $\{8.0 \times 10^{-20}, 4.0 \times 10^{-23}\}$ |
| T | 0.01 s |
| ω | 0.1 rad/s |
| S_w | 0.01 m ² .rad ² /s ³ |
| $\{\sigma_{s_m}^2\}_{m=1}^5$ | 20 m ² |

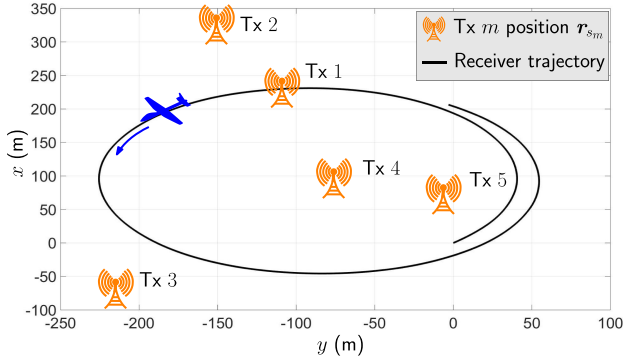


Fig. 2. Simulated environment consisting of $M = 5$ RF transmitters (Tx) (orange) and one UAV-mounted receiver traversing a circular orbit (black).

trajectory [13]. The EKF initialization settings and receiver and RF transmitters' initial states are tabulated in Table III. The environment layout and UAV trajectory is illustrated in Fig. 2. The estimation error trajectories and associated $\pm 2\sigma$ bounds are plotted in Fig. 3(a)–(f) and (g)–(j) for the receiver and RF transmitter 1, respectively.

The following can be concluded from the full system simulation plots in Fig. 3. First, while the variance of $c\tilde{\delta}t_{s_1}$ decreases, at some point in time, it begins to diverge unboundedly. On the other hand, the variance of $c\tilde{\delta}t_r$ starts from zero (due to the prior knowledge about the receiver's clock bias) and diverges unboundedly with time. Second, although the errors $c\tilde{\delta}t_r$ and $c\tilde{\delta}t_s$ are relatively small, their variances will continue to increase and cause the estimation error covariance matrix to become ill-conditioned. Note that an extended information filter (EIF) will not resolve this issue, and a similar problem will be encountered. This is because as the uncertainties of the clock states become larger, the corresponding elements in the information matrix become smaller, causing the information matrix to also

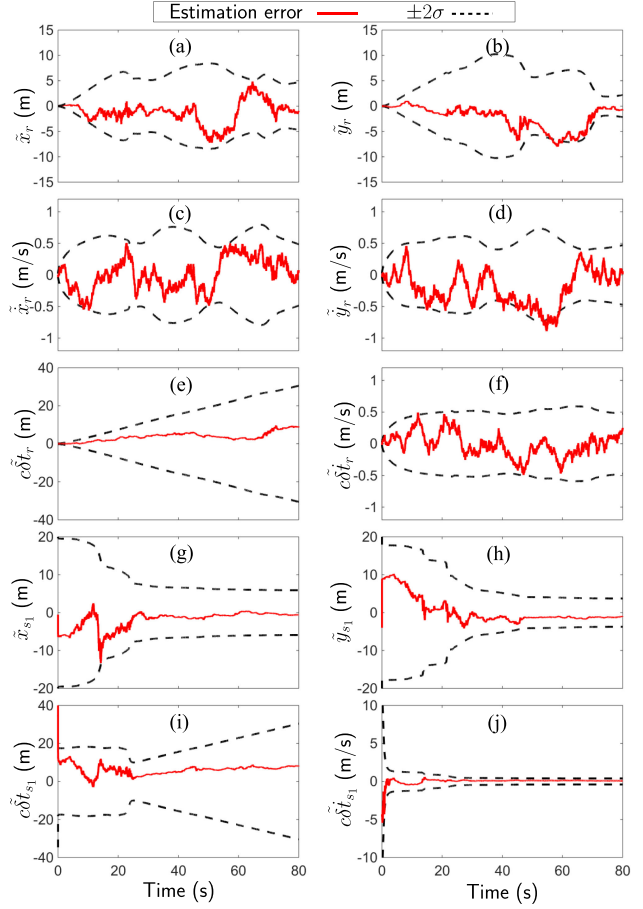


Fig. 3. Estimation error trajectories (red) and corresponding $\pm 2\sigma$ bounds (black) for EKF-based radio SLAM with settings from Table III.

become ill-conditioned. This is evident from the fact that the condition number of the estimation error covariance matrix \mathbf{P} is equal to the condition number of the corresponding information matrix $\mathbf{Y} = \mathbf{P}^{-1}$. Since the pseudorange measurements are a nonlinear function of the receivers' and the RF transmitters' positions, a conversion from the information space to the state space is required in order to compute the measurement residual and the measurement Jacobians, which are necessary for the EIF update step. This conversion requires the inversion of the information matrix which becomes ill-conditioned at the same rate as the covariance matrix. Third, despite the stochastically unobservable clock biases, the estimation error variances appear to have a finite bound for \tilde{x}_r , \tilde{y}_r , \tilde{x}_{s_1} , \tilde{y}_{s_1} , and $c\tilde{\delta}t_{s_1}$. Similar behavior was noted for the estimates associated with the other four RF transmitters.

V. EXPERIMENTAL DEMONSTRATION

A field experiment was conducted in Riverside, CA, USA, using a UAV to demonstrate the stochastically unobservable clock biases of both a UAV-mounted receiver and multiple cellular transmitters when an EKF-based radio SLAM framework is employed.

To this end, a UAV was equipped with a two-channel Ettus E312 universal software radio peripheral (USRP).

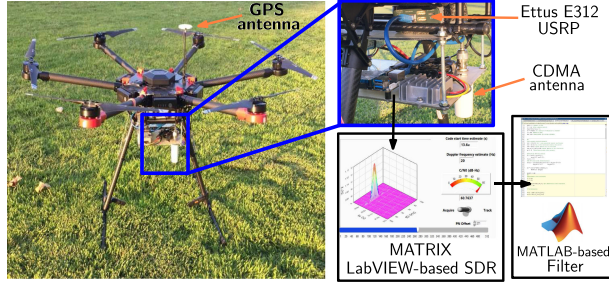


Fig. 4. Experiment hardware setup.

Two antennas were mounted to the UAV and connected to the USRP: 1) a consumer-grade patch GPS antenna and 2) a consumer-grade omni-directional cellular antenna. The USRP was tuned to 1) 1575.42 MHz to sample GPS L1 C/A signals and 2) 882.75 MHz to sample cellular signals, which were modulated through code division multiple access and were transmitted from nearby cellular towers. The E312 fed the sampled data to the multichannel adaptive transceiver information extractor software-defined receiver [31], [32], which produced pseudorange observables to all available GPS SVs and to four cellular towers of the U.S. cellular provider Verizon. The GPS pseudoranges were only used to estimate the UAV-mounted receiver's initial position and clock error states. Such estimates were used to initialize the EKF, which simultaneously estimated the UAV's and the four unknown transmitters' state *before* navigation via radio SLAM began, while cellular pseudoranges were used exclusively *thereafter* as measurements in the EKF. The experimental setup is illustrated in Fig. 4.

The UAV traversed a commanded trajectory for 130 s. The "ground truth" traversed trajectory was obtained from the UAV's onboard integrated navigation system, which used a GPS, an inertial navigation system (INS), and other sensors. The UAV's trajectory was also estimated via the radio SLAM framework described in this paper. The UAV's and cellular towers' heights were assumed to be known for the entire duration of the experiment; therefore, this is a 2-D radio SLAM problem, which is consistent with the stochastic observability analysis conducted in Section III. The EKF-based radio SLAM filter was initialized with a state estimate given by

$$\hat{\mathbf{x}}(0|0) = [\hat{\mathbf{x}}_r^T(0|0), \hat{\mathbf{x}}_{s_1}^T(0|0), \dots, \hat{\mathbf{x}}_{s_4}^T(0|0)]^T$$

and a corresponding estimation error covariance

$$\mathbf{P}(0|0) = \text{diag}[\mathbf{P}_r(0|0), \mathbf{P}_{s_1}(0|0), \dots, \mathbf{P}_{s_4}(0|0)].$$

The UAV-mounted receiver's initial estimate $\hat{\mathbf{x}}_r(0|0)$ was set to the solution provided by the UAV's onboard GPS-INS solution at the beginning of the trajectory, and was assumed to be perfectly known, i.e., $\mathbf{P}_r(0|0) \equiv \mathbf{0}_{6 \times 6}$. The transmitters' initial state estimates were drawn according to $\hat{\mathbf{x}}_{s_m}(0|0) \sim \mathcal{N}([\mathbf{r}_{s_m}^T, \mathbf{x}_{\text{clk}, s_m}^T(0)]^T, \mathbf{P}_{s_m}(0|0))$. The true transmitters' positions $\{\mathbf{r}_{s_m}\}_{m=1}^4$ were surveyed beforehand according to the framework described in [33] and verified

using Google Earth. The initial clock bias and drift

$$\mathbf{x}_{\text{clk}, s_m}(0) = c[\delta t_{s_m}(0), \dot{\delta t}_{s_m}(0)]^T \quad m = 1, \dots, 4$$

were solved for by using the initial set of cellular transmitter pseudoranges (1) according to

$$\begin{aligned} c\delta t_{s_m}(0) &= \|\mathbf{r}_r(0) - \mathbf{r}_{s_m}\| + c\delta t_{r_1}(0) - z_{s_m}(0), \\ c\dot{\delta t}_s(0) &= [c\delta t_s(1) - c\delta t_s(0)]/T, \end{aligned}$$

where $c\delta t_{s_m}(1) = \|\mathbf{r}_r(1) - \mathbf{r}_{s_m}\| + c\delta t_{r_1}(1) - z_{s_m}(1)$. The initial uncertainty associated with the transmitters' states was set to $\mathbf{P}_{s_m}(0|0) \equiv 10^3 \cdot \text{diag}[1, 1, 3, 0.3]$ for $m = 1, \dots, 4$.

The process noise covariance of the receiver's clock $\mathbf{Q}_{\text{clk}, r}$ was set to correspond to a typical temperature-compensated crystal oscillator with $h_{0, r} = 9.4 \times 10^{-20}$ and $h_{-2, r} = 3.8 \times 10^{-21}$. The process noise covariances of the cellular transmitters' clocks were set to correspond to a typical oven-controlled crystal oscillator with $h_{0, s_m} = 8 \times 10^{-20}$ and $h_{-2, s_m} = 4 \times 10^{-23}$, which is usually the case for cellular transmitters [34], [35]. The UAV's position and velocity states were assumed to evolve according to velocity random walk dynamics with

$$\begin{aligned} \mathbf{f}_{\text{pv}}[\mathbf{x}_{\text{pv}}(k)] &= \begin{bmatrix} \mathbf{I}_{2 \times 2} & T\mathbf{I}_{2 \times 2} \\ \mathbf{0}_{2 \times 2} & \mathbf{I}_{2 \times 2} \end{bmatrix} \mathbf{x}_{\text{pv}}(k), \\ \mathbf{Q}_{\text{pv}} &= \begin{bmatrix} \frac{T^3}{3}\mathbf{S}_{\text{pv}} & \frac{T^2}{2}\mathbf{S}_{\text{pv}} \\ \frac{T^2}{2}\mathbf{S}_{\text{pv}} & T\mathbf{S}_{\text{pv}} \end{bmatrix}, \end{aligned}$$

where $T = 0.0267$ s and $\mathbf{S}_{\text{pv}} = \text{diag}[0.02, 0.2]$ is the process noise power spectral density matrix, whose value was found empirically. The measurement noise variances $\{\sigma_{s_m}^2\}_{m=1}^4$ were computed beforehand according to the method described in [33], and were found to be $\sigma_{s_1}^2 = 0.7$, $\sigma_{s_2}^2 = 0.2$, $\sigma_{s_3}^2 = 0.7$, and $\sigma_{s_4}^2 = 0.1$. The trajectory produced by the UAV's onboard integrated GPS-INS and the one estimated by the radio SLAM framework are plotted in Fig. 5 along with the initial uncertainty ellipses of the four transmitters and the final east-north 99th-percentile estimation uncertainty ellipses for tower 1. Similar reduction in the final uncertainty ellipses corresponding to the three other towers was noted.

The root mean squared error of the UAV's estimated trajectory was 9.5 m and the final error was 7.9 m. These errors were computed with respect to the GPS-INS trajectory. The resulting estimation errors and corresponding $\pm 2\sigma$ bounds of the vehicle's east and north position and the $\pm 2\sigma$ bounds of the clock bias of both the receiver and tower 1 are plotted in Fig. 6. Only the $\pm 2\sigma$ bounds are shown for the clock biases of both the receiver and tower 1, since the true biases are unknown; therefore, the estimation error trajectories cannot be plotted. Note that while the estimation error variances of the UAV's east and north position remained bounded, the estimation error variances of the receiver and tower 1 grew unboundedly, indicating their stochastic unobservability, which is consistent with the simulation results presented in Section IV and Theorem III.1.

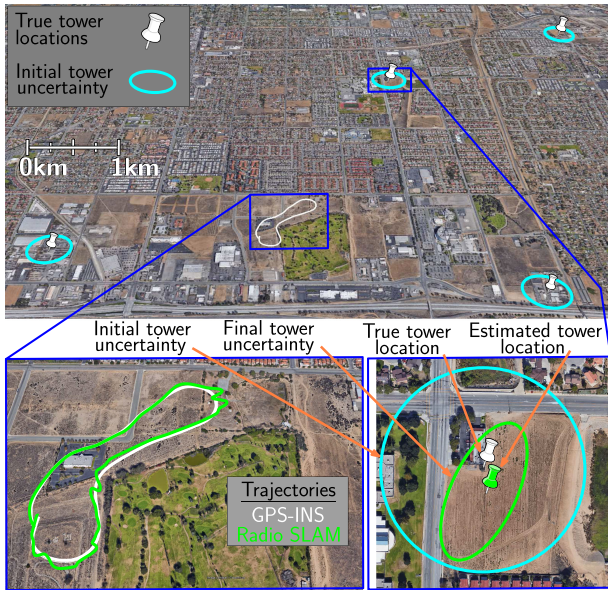


Fig. 5. Environment layout and experimental results showing the estimated UAV trajectories from (a) its onboard GPS-INS integrated navigation system (white) and (b) radio SLAM (green), the initial position uncertainty of each unknown tower, and tower 1 final position estimate and corresponding uncertainty ellipse. Image: Google Earth.

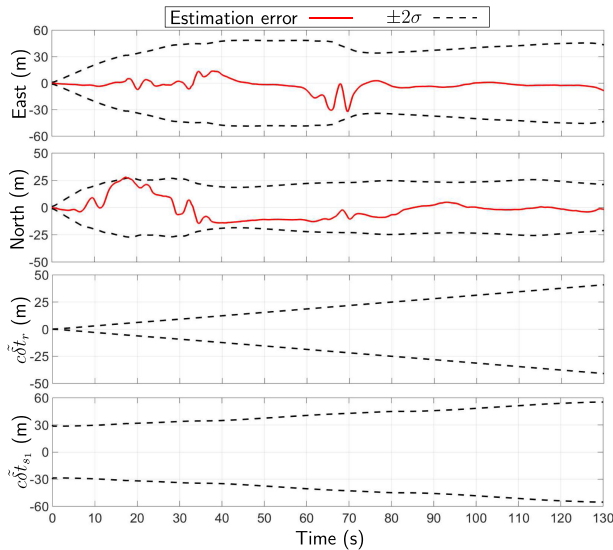


Fig. 6. Radio SLAM experimental results: north and east errors of the UAV-mounted receiver and corresponding estimation error variances and the estimation error variances of the clock bias for both the receiver and transmitter 1.


VI. CONCLUSION

The stochastic observability of a simultaneous receiver localization and transmitter mapping problem was studied. It was demonstrated that the system is stochastically unobservable when the clock biases of both a receiver and unknown transmitters are simultaneously estimated and that their associated estimation error variances will diverge. The divergence rate of a sequence lower-bounding the diverging variances was derived and shown to reach a steady-state that only depends on the receiver's clock

quality. Despite the stochastically unobservable clock biases, simulation and experimental results demonstrated bounded localization errors of a UAV navigating via radio SLAM for 130 s without GPS.

ACKNOWLEDGMENT

The authors would like to thank J. Khalife for his help with data collection.

JOSHUA J. MORALES, *Student Member, IEEE*
ZAHER (ZAK) M. KASSAS , *Senior Member, IEEE*
 University of California, Riverside USA
 E-mail: (jmora047@ucr.edu; zkassas@ieee.org)

REFERENCES

- [1] A. Dempster and E. Cetin, "Interference localization for satellite navigation systems," *Proc. IEEE*, vol. 104, no. 6, pp. 1318–1326, Jun. 2016.
- [2] M. Psiaki and T. Humphreys, "GNSS spoofing and detection," *Proc. IEEE*, vol. 104, no. 6, pp. 1258–1270, Jun. 2016.
- [3] J. Raquet and R. Martin, "Non-GNSS radio frequency navigation," In *Proc. IEEE Int. Conf. Acoust., Speech Signal Process.*, Mar. 2008, pp. 5308–5311.
- [4] Z. Kassas, "Collaborative opportunistic navigation," *IEEE Aerospace Electron. Syst. Mag.*, vol. 28, no. 6, pp. 38–41, Jun. 2013.
- [5] J. McEllroy, "Navigation using signals of opportunity in the AM transmission band," Master's thesis, Air Force Institute of Technology, Wright-Patterson Air Force Base, OH, USA, 2006.
- [6] C. Yang, T. Nguyen, and E. Blasch, "Mobile positioning via fusion of mixed signals of opportunity," *IEEE Aerospace Electron. Syst. Mag.*, vol. 29, no. 4, pp. 34–46, Apr. 2014.
- [7] Z. Kassas, J. Khalife, K. Shamaei, and J. Morales, "I hear, therefore I know where I am: Compensating for GNSS limitations with cellular signals," *IEEE Signal Process. Mag.*, pp. 111–124, Sep. 2017.
- [8] M. Rabinowitz and J. Spilker, Jr., "A new positioning system using television synchronization signals," *IEEE Trans. Broadcasting*, vol. 51, no. 1, pp. 51–61, Mar. 2005.
- [9] P. Thevenon *et al.*, "Positioning using mobile TV based on the DVB-SH standard," *Navigation, J. Institute Navigation*, vol. 58, no. 2, pp. 71–90, 2011.
- [10] K. Pesyna, Z. Kassas, and T. Humphreys, "Constructing a continuous phase time history from TDMA signals for opportunistic navigation," In *Proc. IEEE/ION Position Location Navigation Symp.*, Apr. 2012, pp. 1209–1220.
- [11] M. Leng, F. Quitin, W. Tay, C. Cheng, S. Razul, and C. See, "Anchor-aided joint localization and synchronization using SOOP: Theory and experiments," *IEEE Trans. Wireless Commun.*, vol. 15, no. 11, pp. 7670–7685, Nov. 2016.
- [12] Z. Kassas, "Analysis and synthesis of collaborative opportunistic navigation systems," Ph.D. dissertation, The University of Texas at Austin, Austin, TX, USA, 2014.

- [13] Z. Kassas, A. Arapostathis, and T. Humphreys
Greedy motion planning for simultaneous signal landscape mapping and receiver localization
IEEE J. Select. Topics Signal Process., vol. 9, no. 2, pp. 247–258, Mar. 2015.
- [14] H. Durrant-Whyte and T. Bailey
Simultaneous localization and mapping: Part I
IEEE Robot. Autom. Mag., vol. 13, no. 2, pp. 99–110, Jun. 2006.
- [15] J. Andrade-Cetto and A. Sanfeliu
The effects of partial observability when building fully correlated maps
IEEE Trans. Robot., vol. 21, no. 4, pp. 771–777, Aug. 2005.
- [16] T. Vida-Calleja, M. Bryson, S. Sukkarieh, A. Sanfeliu, and J. Andrade-Cetto
On the observability of bearing-only SLAM
In *Proc. IEEE Int. Conf. Robot. Autom.*, Apr. 2007, vol. 1, pp. 4114–4118.
- [17] Z. Wang and G. Dissanayake
Observability analysis of SLAM using Fisher information matrix
In *Proc. IEEE Int. Conf. Control, Autom., Robot. Vision*, Dec. 2008, vol. 1, pp. 1242–1247.
- [18] M. Bryson and S. Sukkarieh
Observability analysis and active control for airborne SLAM
IEEE Trans. Aerospace Electron. Syst., vol. 44, no. 1, pp. 261–280, Jan. 2008.
- [19] Z. Kassas and T. Humphreys
Observability analysis of collaborative opportunistic navigation with pseudorange measurements
IEEE Trans. Intell. Transp. Syst., vol. 15, no. 1, pp. 260–273, Feb. 2014.
- [20] Z. Kassas and T. Humphreys
Receding horizon trajectory optimization in opportunistic navigation environments
IEEE Trans. Aerospace Electron. Syst., vol. 51, no. 2, pp. 866–877, Apr. 2015.
- [21] V. Bageshwar, D. Gebre-Egziabher, W. Garrard, and T. Georgiou
Stochastic observability test for discrete-time Kalman filters
J. Guidance, Control, Dyn., vol. 32, no. 4, pp. 1356–1370, Jul. 2009.
- [22] H. Chen
Recursive Estimation and Control for Stochastic Systems. New York, NY, USA: Wiley, 1985.
- [23] Y. Baram and T. Kailath
Estimability and regulability of linear systems
IEEE Trans. Autom. Control, vol. 33, no. 12, pp. 1116–1121, Dec. 1988.
- [24] K. Reif, S. Gunther, E. Yaz, and R. Unbehauen
Stochastic stability of the discrete-time extended Kalman filter
IEEE Trans. Autom. Control, vol. 44, no. 4, pp. 714–728, Apr. 1999.
- [25] K. Reif, S. Gunther, E. Yaz, and R. Unbehauen
Stochastic stability of the continuous-time extended Kalman filter
IEE Proc. - Control Theory Appl., vol. 147, no. 1, pp. 45–52, Jan. 2000.
- [26] Y. Bar-Shalom, X. Li, and T. Kirubarajan
Estimation With Applications to Tracking and Navigation. New York, NY, USA: Wiley, 2002.
- [27] A. Liu
Stochastic observability, reconstructibility, controllability, and reachability
Ph.D. dissertation, University of California, San Diego, CA, USA, 2011.
- [28] A. Thompson, J. Moran, and G. Swenson
Interferometry and Synthesis in Radio Astronomy, 2nd ed. Hoboken, NJ, USA: Wiley, 2001.
- [29] X. Li and V. Jilkov
Survey of maneuvering target tracking. Part I: Dynamic models
IEEE Trans. Aerospace Electron. Syst., vol. 39, no. 4, pp. 1333–1364, Oct. 2003.
- [30] J. Mendel
Lessons in Estimation Theory for Signal Processing, Communications, and Control, 2nd ed. Englewood Cliffs, NJ, USA: Prentice-Hall, 1995.
- [31] J. Khalife, K. Shamaei, and Z. Kassas
A software-defined receiver architecture for cellular CDMA-based navigation
In *Proc. IEEE/ION Position, Location, Navigation Symp.*, Apr. 2016, pp. 816–826.
- [32] Z. Kassas, J. Morales, K. Shamaei, and J. Khalife
LTE steers UAV
GPS World Mag., vol. 28, no. 4, pp. 18–25, Apr. 2017.
- [33] J. Morales and Z. Kassas
Optimal collaborative mapping of terrestrial transmitters: receiver placement and performance characterization
IEEE Trans. Aerospace Electron. Syst., vol. 54, no. 2, pp. 992–1007, Apr. 2018.
- [34] K. Pesyna, Z. Kassas, J. Bhatti, and T. Humphreys
Tightly-coupled opportunistic navigation for deep urban and indoor positioning
In *Proc. ION GNSS Conf.*, Sep. 2011, pp. 3605–3617.
- [35] Z. Kassas, V. Ghadiok, and T. Humphreys
Adaptive estimation of signals of opportunity
In *Proc. ION GNSS Conf.*, Sep. 2014, pp. 1679–1689.